PHYSICAL REVIEW RESEARCH **2**, 012065(R) (2020)

Rapid Communications

Magnetic-field-induced transition in a quantum dot coupled to a superconductor

A. García Corral,[1] D. M. T. van Zanten,[1,*] K. J. Franke,[2] H. Courtois,[1] S. Florens,[1] and C. B. Winkelmann[1,†]

[1]*Univ. Grenoble Alpes, CNRS, Grenoble INP, Institut Néel, 38000 Grenoble, France*

[2]*Fachbereich Physik, Freie Universität Berlin, 14195 Berlin, Germany*

(Received 11 December 2019; revised manuscript received 25 February 2020; accepted 26 February 2020; published 16 March 2020)

The magnetic moment of a quantum dot can be screened by its coupling to a superconducting reservoir, depending on the hierarchy of the superconducting gap and the relevant Kondo scale. This screening-unscreening transition can be driven by electrostatic gating, tunnel coupling, and, as we demonstrate here, a magnetic field. We perform high-resolution spectroscopy of subgap excitations near the screening-unscreening transition of asymmetric superconductor-quantum dot-superconductor (S–QD–S) junctions formed by the electromigration technique. Our measurements reveal a re-entrant phase boundary determined by the competition between Zeeman energy and gap reduction with magnetic field. We further track the evolution of the phase transition with increasing temperature, which is also evinced by thermal replicas of subgap states.

DOI: 10.1103/PhysRevResearch.2.012065

The junction between a superconductor and a quantum dot displays discrete subgap energy levels called Andreev bound states (ABSs) or, more specifically, Yu-Shiba-Rusinov (YSR) states when the highest occupied level hosts a single spin [1–3]. When the antiferromagnetic exchange interaction between this spin and the leads prevails over the superconducting gap Δ, the localized spin is effectively Kondo screened, and a quasiparticle is bound at the interface. In contrast, if the exchange coupling is weaker, the superconducting condensate is marginally perturbed and the spin remains unscreened. The change between these two distinct ground states occurs via a sharp level crossing, which constitutes a simple realization of a quantum phase transition. In recent years, detailed investigations of this screening-unscreening transition have been performed, using as a control knob the variation of the level depth [4–11], the superconducting phase difference [12], or the tunnel coupling, which effectively modifies the exchange coupling strength [13–16]. The variation of an external magnetic field may provide an additional parameter with twofold consequences: increasing the magnetic field suppresses superconducting correlations (hence favoring a screened state), while the Zeeman effect enhances polarization towards one of the magnetic YSR states [9,10,17,18]. Thus, the two effects associated with a magnetic field lead to a shifting of level crossing in opposite directions.

Experimentally, it is challenging to explore the effect of the magnetic field on the screening-unscreening transition, precisely for the reason that superconductivity is usually quenched before the quantum phase transition can be accessed. Hence, the quantum dot systems needs to be tuned close to the critical point using another control parameter, here the back-gate voltage allowed in our transistor geometry. Furthermore, the detection of tiny level shifts between subgap states requires exquisite energy resolution in the μV range, which can be achieved only with superconducting leads.

In this Rapid Communication, we report on the observation of the magnetic field-controlled screened-unscreened ground-state transition of a quantum dot strongly coupled to one superconducting lead. An asymmetrically coupled superconductor-quantum dot-superconductor (S–QD–S) device combines the gate tunability of single-electron transistors with the unprecedented spectroscopic resolution of the subgap states. Monitoring the dispersion of the subgap states allows tracking the transition between the screened and unscreened spin ground states of the quantum dot as a function of the bare level of the dot, temperature, and, most importantly, magnetic field. We use the Anderson impurity as the main framework for the modelization of our data. A general phase diagram is drawn, which demonstrates a striking re-entrant behavior of the phase boundary, due to the previously mentioned competition between Zeeman splitting and superconducting gap closing. In addition, thermal replicas of YSR states are found to emerge at finite temperature, providing an alternative yet consistent picture of the subgap spectrum.

The device fabrication process relies on controlled electromigration of an on-chip all-metallic aluminum device presenting a constriction [19]. This technique produces nanometer sized gaps and was successfully applied for connecting single molecules [20–23]. Electrostatic gate control is provided through a local metallic back gate isolated by a 18-nm-thick ZrO_2 dielectric layer. Using aluminum as the constriction material, gated S–QD–S devices can thereby be formed [24–26].

*Present address: Center for Quantum Devices, Niels Bohr Institute, University of Copenhagen, and Microsoft Quantum Lab Copenhagen, Denmark.

†Corresponding author: clemens.winkelmann@neel.cnrs.fr

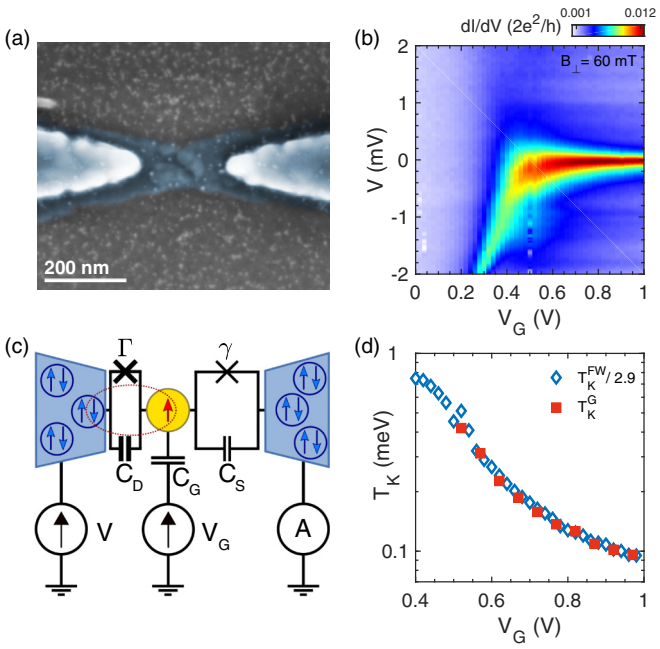

FIG. 1. (a) Scanning electron micrograph of a nanoparticle-covered Al constriction after electromigration. (b) Normal state dI/dV differential conductance map of device A at a base temperature of $T = 100$ mK, for a magnetic field $B = 60$ mT suppressing superconductivity. (c) Schematics of the S–QD–S device, introducing the three capacitances and two tunnel couplings at play. (d) Experimental gate dependence of the Kondo energy scale T_K, determined from the temperature dependence of the linear conductance (red squares), as well as by a rescaling with a dividing factor 2.9 of the FWHM of the low-bias conductance peak (blue open diamonds).

Our quantum dots are colloidal gold nanoparticles of 5 nm diameter. Electromigration is performed at 4.2 K in cryogenic vacuum in a dilution cryostat. A scanning electron micrograph of an Al constriction after electromigration (without nanoparticles, for better visibility) is shown in Fig. 1(a). Samples showing stable gate-dependent conductance features are further investigated at temperatures down to $T = 80$ mK. The differential conductance $G(V, V_G) = dI/dV$ is measured by using the lock-in technique, as a function of bias V and gate voltage V_G. We show here data mostly from one sample, labeled A. Data from a second and similar sample (B) can be found in the Supplemental Material [27].

The normal-state differential conductance map (obtained at a magnetic field of 60 mT) is shown in Fig. 1(b), around the only experimentally accessible degeneracy point at $V_G^0 \approx 0.40$ V. The Kondo resonance is unaffected by magnetic up to fields of 120 mT (see Supplemental Material, Fig. S4). To the left, the linear conductance is suppressed, owing to a Coulomb-blockaded state with an even electron occupation number N. As the gate voltage V_G is increased, a zero-bias resonance indicates the onset of Kondo correlations associated with the spin-1/2 degeneracy of the oddly occupied $N + 1$ electron state. The electrical model of the quantum dot junction is displayed in Fig. 1(c). The tunnel couplings to both leads are strongly asymmetric ($\Gamma \gg \gamma$), as evidenced by a nonunitary linear conductance limit, $G(T \to 0)/(2e^2/h) = 4\Gamma\gamma/(\Gamma + \gamma)^2 \approx 0.013$ (see Supplemental Material [27]). This implies notably that the Kondo resonance builds between the QD and the drain electrode at experimentally accessible temperatures, the source contact acting as a tunnel probe, as is usually the case for the tip in a scanning tunneling microscopy experiment. The following values of hybridization $\Gamma = 1.4$ meV (implying $\gamma = 5$ μeV) and Coulomb repulsion $U = 12.6$ meV in the quantum dot are found from fits of the gate-dependent zero-bias conductance to numerical renormalization group (NRG) calculations (see Supplemental Material [27]). The ratio $U/\Gamma \simeq 9$ shows that the quantum dot is in the strongly correlated regime, with some deviations from Kondo scaling.

The full width at half maximum (FWHM) of the conduction resonance at the Fermi level, as shown in Fig. 1(b), is often taken as an approximate measure of the Kondo temperature T_K, that we note T_K^{FW} (here and later we set $k_B = 1$, identifying temperature and energy scales). Another direct and precise determination of T_K is achieved considering the measured temperature dependence of the linear conductance $G(T)$. The latter can be fit by NRG calculations, or for a lower computational cost, by an empirical expression [42,43], leading to the gate-dependent Kondo temperature denoted T_K^G shown in Fig. 1(d) (see also Supplemental Material [27]). We find that these estimates agree closely within a scaling factor, such that $T_K^G = T_K^{\mathrm{FW}}/2.9$. Therefore, it is seen that the quantum dot junction behaves like a single spin-1/2 Kondo impurity, with a gate-tunable T_K that can be brought to the same order of magnitude as the superconducting order parameter of the leads, leading to a standard gate control of the screening transition [44,45].

We now turn to the study of the S–QD–S transistor at zero magnetic field. In presence of superconductivity in both leads, a transport gap of total width $2(\Delta + \Delta_{\mathrm{probe}}) \approx 900$ μeV opens in the transport map, see Fig. 2(b). The Kondo peak is suppressed and two sharp symmetric resonances appear at a certain biasing voltage V so that $0 < |eV| - \Delta_{\mathrm{probe}} < \Delta$. We take care to differentiate the gap $\Delta \approx 245$ μeV of the strongly coupled lead, which governs the physical effects at play, from the gap $\Delta_{\mathrm{probe}} \approx 205$ μeV of the weakly coupled electrode, which offsets essentially the conductance onset thresholds by $\pm\Delta_{\mathrm{probe}}$. Thermal excitations at 940 mK, which will be discussed further below, provide unambiguous evidence of the probe's gap size [see Fig. 4(a)].

The presence of the YSR states is reflected by extremely sharp subgap resonances [Fig. 2(a)] at $|eV| = |E_B| + \Delta_{\mathrm{probe}}$; that is, when the probe's chemical potential allows for driving the dot to its excited state by either adding or removing an electron. The transport mechanisms leading to a dc current here are essentially based on Andreev processes [46]. From the experimental gate dependence of the bound-state spectrum E_B, the singlet-doublet ground-state transition, occurring for $E_B = 0$, is readily seen to occur near $V_G = 0.71$ V. Note that, owing to the very sharply defined gap edge of aluminum [25], but also low experimental temperatures and careful shielding of the experiment, we can achieve a spectroscopic resolution down to a FWHM of less than 10 μeV [Fig. 2(a)], way below previously reported linewidths [13,47–49]. The latter have indeed been discussed as a lifetime limiting factor in possible subgap state-based qubits [6,50].

Combining our knowledge of the superconducting- and normal-state properties, we can now plot the bound-state

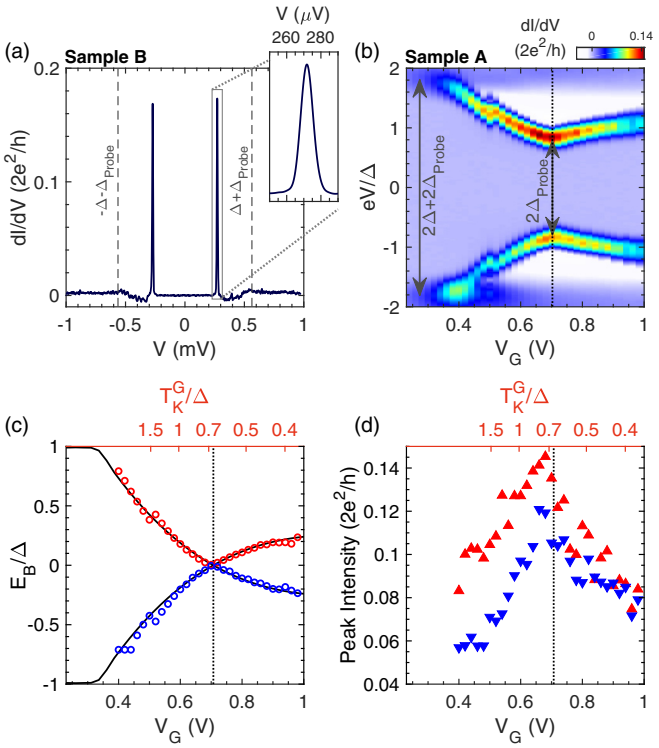

FIG. 2. (a) Differential conductance of device B measured with a lock-in ac oscillation of 2 μV in the superconducting state at fixed $V_G = 0.5$ V, displaying very-sharply-resolved YSR resonances, with a FWHM = 9 μV (see inset). (b) Gate-dependent differential conductance of device A in the superconducting state at a base temperature of $T = 80$ mK, revealing the dispersion of the YSR states. The minimal spacing of the two resonances, given by a voltage span $2\Delta_{\text{probe}}/e$ with $\Delta_{\text{probe}} = 205$ μeV, is associated with the quantum ground-state transition, occurring at $V_G = 0.71$ V. (c) Extracted bound state energy E_B versus gate V_G and dimensionless theoretical Kondo temperature T_K^{th}/Δ, in comparison to theoretical predictions (lines). The dashed vertical line indicates the ground-state transition, found at $T_K^{\text{th}}/\Delta \approx 0.26$. (d) Evolution of the conductance peak intensities with V_G, showing a kink at the transition, consistent with a sharp unscreening transition.

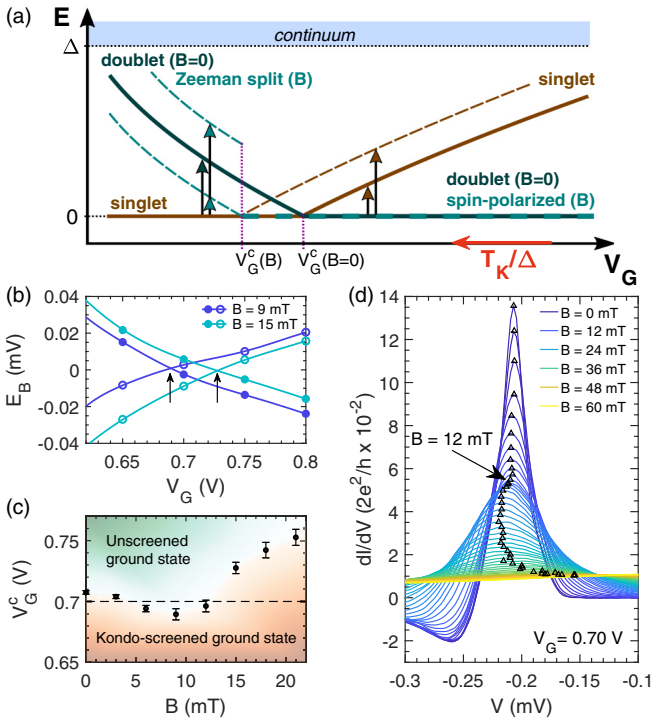

FIG. 3. (a) Sketch of level structure of YSR states at zero magnetic field (continuous lines) and finite (dashed lines) magnetic field, in vicinity of the ground-state transition. (b) Zoom on the zero-energy crossings of the bound-state dispersion for two magnetic-field values, $B = 9$ and 15 mT (symbols). The solid lines are a spline interpolation of the data, from the crossing of which the value of the critical gate voltage V_G^c is determined (arrows). (c) Phase diagram of the screening transition in (V_G, B) space, showing a re-entrant phase boundary. (d) Spectroscopic analysis of the YSR states as a function of bias and at a fixed gate voltage of $V_G = 0.70$ V, close to the zero-field critical point at $V_G^c = 0.71$ V. By increasing the magnetic field, a sharp kink is seen indicating the re-entrant phase boundary at $B = 12$ mT.

dispersion E_B as a function of gate voltage V_G, which we express as a function of the dimensionless ratio T_K^G/Δ [Fig. 2(c)]. We find the transition to the unscreened ground state for the critical value $(T_K^G/\Delta)_c \simeq 0.7$ consistent with Ref. [51] or with the value $(T_K^{\text{FW}}/2\Delta)_c \simeq 1.0$ in Ref. [52]. Theoretical calculations [44] predict a critical value $(T_K^{\text{th}}/\Delta)_c \simeq 0.30$, using the scaling formula $T_K^{\text{th}} \simeq 0.28\sqrt{U\Gamma}\exp[\pi\epsilon_0(\epsilon_0+U)/(2\Gamma)]$. While we can rescale our data to T_K^{th} (for instance at the value at the center of the diamond), which gives a reasonable value $(T_K^{\text{th}}/\Delta)_c \simeq 0.26$, we emphasize that our device is not strictly in the scaling regime where these predictions apply quantitatively [53]. In addition, a calculation using renormalized ABS theory [54] allows us to obtain a full gate-dispersion of the bound state in good agreement with the experimental observation; see Fig. 2(c) and the Supplemental Material [27] for details. Furthermore, the intensities of the conductance peaks, which reflect the weights carried by bound states, also follow the expected behavior [44] across the ground-state transition, as shown in Fig. 2(d).

Having understood in detail the zero-field properties of the QD–S hybrid, we now move to the main result of this work, in which we evince the competition of two magnetic effects on the ground-state transition of the quantum dot. A magnetic field B is expected to Zeeman split the two spin projections of the doublet state by $E_Z = \pm g\mu_B B/2$, with g being the gyromagnetic factor and μ_B the Bohr magneton. The effect of the Zeeman splitting on the doublet state has been observed in superconductor-quantum dot junctions formed in semiconducting nanowires, owing to the large $g \approx 20$ in these materials [9,10,17]. In these works, the subgap resonances are Zeeman split at the singlet ground-state phase because two excited states are accessible. In contrast, when the singlet is the excited state, no splitting was seen, because the only possible transition (at low temperature $T < E_Z$) is from the lower-energy spin-polarized state to the singlet.

Beyond the mere spectroscopic effect of the Zeeman splitting of the doublet excited state at a given dot level depth, we now consider the magnetic-field effect on the ground-state transition itself. Indeed, because one of the spin

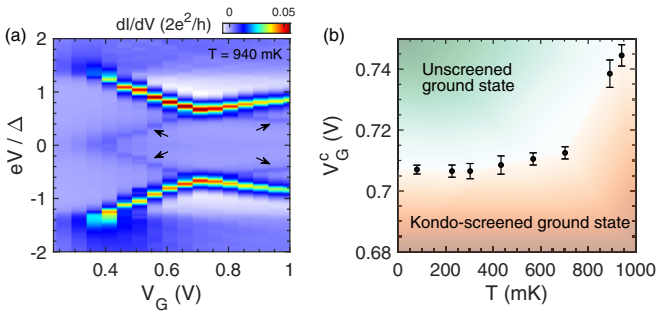

FIG. 4. (a) Differential conductance of device A in the superconducting state at the higher temperature $T = 940\,\mathrm{mK}$, displaying the YSR resonances and their thermal replicas (black arrows). (b) Gate dependence of the YSR states at 940 mK, as found from the main conductance resonances (similar data are found from the thermal replicas). Owing to the temperature-driven reduction of the superconducting gap Δ, the ground-state transition has moved to the larger critical gate voltage $V_G^c \approx 0.74\,\mathrm{V}$ at the largest measured temperature.

projections of the unscreened spin state has a lower energy, the screened ground-state phase space gradually shrinks, which is translated here into a critical value of V_G moving to lower values. This is sketched in Fig. 3(a) and precisely observed in Fig. 3(c), where we plot the critical gate value V_G^c associated with the ground-state transition as a function of magnetic field. The latter is determined as previously from the kink (crossing) in the YSR dispersion, for each applied magnetic field as shown in Fig. 3(b). For small fields $B < 10\,\mathrm{mT}$, there is a clear downward trend of V_G^c, indicating a Zeeman-driven reduction of the parameter space associated with the singlet ground state. As the magnetic field is further increased, the reduction of the superconducting gap starts coming into play, with a quadratic magnetic field dependence of the gap to lowest order [55]. Intuitively, the gradual weakening of superconductivity favors Kondo screening of the spin in the dot, and thereby favors the singlet ground state, enhancing again the critical V_G^c [Fig. 3(c)]. This re-entrance of the phase-boundary is confirmed when sweeping the magnetic field at a fixed gate voltage $V_G = 0.70\,\mathrm{V}$ [Fig. 3(d)]. The transition of the ground-state parity induced near a field of 12 mT is accompanied by an abrupt change in the YSR spectra, which move to higher energies and acquire a broader lineshape (see Supplemental Material for details [27]).

For completeness, we finally focus on the effect of higher temperatures for the tunnelling spectroscopies as well as the ground-state transition. First, at higher temperatures, the nonzero probability of finding the dot in its excited state allows for new conductance resonances in tunneling spectroscopies emerging at $|eV| = \Delta_{\mathrm{probe}} - |E_B|$, which are commonly referred to as *thermal replicas* of the YSR resonances [7,13]. This is readily seen as a pair of new peaks at low voltages in Fig. 4(a). The corresponding values of the bound-state energy E_B can now also be deduced from the related supplementary threshold conditions, in excellent agreement with the bound-state energies deduced from the *main* resonances, leading to the data shown in Fig. 4(b). The singlet-doublet transition can thus be equally observed from the thermal replicas. Second, the thermal weakening of the superconducting gap provides another method for tuning the singlet-doublet ground-state transition. At $T = 940\,\mathrm{mK}$, we indeed find that the transition has moved to a larger gate value, about $V_G^c \simeq 0.74\,\mathrm{V}$ (or equivalently at a lower T_K than for the base temperature), in agreement with expectations. Obviously, no re-entrance is observed in the temperature dependence of the transition.

In conclusion, we have demonstrated a magnetic-field tuning of the screening-unscreening transition of a quantum dot coupled to superconductors in a transistor geometry. A novel phase diagram was established, demonstrating that the magnetic field leads to a re-entrant transition due to the competition between Zeeman stabilization of the lowest spin-polarized orbital and weakening of the superconducting gap. A complementary finite-temperature phase diagram was drawn, which reflects the sole thermal weakening on the superconducting gap, while signatures of the ground-state transition were also observed in thermally excited replicas. These results demonstrate that quantum dots constitute a rich model system for the controlled exploration of strong correlations effects in nanostructures. Further developments will address the influence of the screening-unscreening transition on operational properties of single-electron turnstiles [26].

This work was funded by the joint ANR-DFG grant JOSPEC (ANR-17-CE30-0030) and the Labex LANEF programme (ANR-10-LABX-51-01). Samples were fabricated at the Nanofab facility at Institut Néel-CNRS and PTA-CEA. We thank D. Basko, J. Pekola, N. Hatter, and B. Heinrich for useful discussions.

[1] A. V. Balatsky, I. Vekhter, and J.-X. Zhu, Impurity-induced states in conventional and unconventional superconductors, Rev. Mod. Phys. **78**, 373 (2006).

[2] S. De Franceschi, L. Kouwenhoven, C. Schönenberger, and W. Wernsdorfer, Hybrid superconductor–quantum dot devices, Nat. Nanotechnol. **5**, 703 (2010).

[3] B. W. Heinrich, J. I. Pascual, and K. J. Franke, Single magnetic adsorbates on *s*-wave superconductors, Prog. Surf. Sci. **93**, 1 (2018).

[4] M. R. Buitelaar, T. Nussbaumer, and C. Schönenberger, Quantum Dot in the Kondo Regime Coupled to Superconductors, Phys. Rev. Lett. **89**, 256801 (2002).

[5] R. S. Deacon, Y. Tanaka, A. Oiwa, R. Sakano, K. Yoshida, K. Shibata, K. Hirakawa, and S. Tarucha, Tunneling Spectroscopy of Andreev Energy Levels in a Quantum Dot Coupled to a Superconductor, Phys. Rev. Lett. **104**, 076805 (2010).

[6] J.-D. Pillet, C. H. L. Quay, P. Morfin, C. Bena, A. Levy Yeyati, and P. Joyez, Andreev bound states in supercurrent-carrying carbon nanotubes revealed, Nat. Phys. **6**, 965 (2010).

[7] E. J. H. Lee, X. Jiang, R. Aguado, G. Katsaros, C. M. Lieber, and S. De Franceschi, Zero-Bias Anomaly in a Nanowire Quantum Dot Coupled to Superconductors, Phys. Rev. Lett. **109**, 186802 (2012).

[8] J.-D. Pillet, P. Joyez, R. Žitko, and M. F. Goffman, Tunneling spectroscopy of a single quantum dot coupled to a superconductor: From Kondo ridge to Andreev bound states, Phys. Rev. B **88**, 045101 (2013).

[9] E. J. Lee, X. Jiang, M. Houzet, R. Aguado, C. M. Lieber, and S. De Franceschi, Spin-resolved Andreev levels and parity crossings in hybrid superconductor-semiconductor nanostructures, Nat. Nanotechnol. **9**, 79 (2014).

[10] A. Jellinggaard, K. Grove-Rasmussen, M. H. Madsen, and J. Nygård, Tuning Yu-Shiba-Rusinov states in a quantum dot, Phys. Rev. B **94**, 064520 (2016).

[11] A. Assouline, C. Feuillet-Palma, A. Zimmers, H. Aubin, M. Aprili, and J.-C. Harmand, Shiba Bound States across the Mobility Edge in Doped InAs Nanowires, Phys. Rev. Lett. **119**, 097701 (2017).

[12] R. Delagrange, D. J. Luitz, R. Weil, A. Kasumov, V. Meden, H. Bouchiat, and R. Deblock, Manipulating the magnetic state of a carbon nanotube Josephson junction using the superconducting phase, Phys. Rev. B **91**, 241401(R) (2015).

[13] K. J. Franke, G. Schulze, and J. I. Pascual, Competition of superconducting phenomena and Kondo screening at the nanoscale, Science **332**, 940 (2011).

[14] J. O. Island, R. Gaudenzi, J. de Bruijckere, E. Burzurí, C. Franco, M. Mas-Torrent, C. Rovira, J. Veciana, T. M. Klapwijk, R. Aguado, and H. S. J. van der Zant, Proximity-Induced Shiba States in a Molecular Junction, Phys. Rev. Lett. **118**, 117001 (2017).

[15] L. Farinacci, G. Ahmadi, G. Reecht, M. Ruby, N. Bogdanoff, O. Peters, B. W. Heinrich, F. von Oppen, and K. J. Franke, Tuning the Coupling of an Individual Magnetic Impurity to a Superconductor: Quantum Phase Transition and Transport, Phys. Rev. Lett. **121**, 196803 (2018).

[16] L. Malavolti, M. Briganti, M. Hänze, G. Serrano, I. Cimatti, G. McMurtrie, E. Otero, P. Ohresser, F. Totti, M. Mannini, R. Sessoli, and S. Loth, Tunable spin-superconductor coupling of spin 1/2 vanadyl phtalocyanine molecules, Nano Lett. **18**, 7955 (2018).

[17] S. Li, N. Kang, P. Caroff, and H. Q. Xu, 0–π phase transition in hybrid superconductor–InSb nanowire quantum dot devices, Phys. Rev. B **95**, 014515 (2017).

[18] L. Cornils, A. Kamlapure, L. Zhou, S. Pradhan, A. A. Khajetoorians, J. Fransson, J. Wiebe, and R. Wiesendanger, Spin-Resolved Spectroscopy of the Yu-Shiba-Rusinov States of Individual Atoms, Phys. Rev. Lett. **119**, 197002 (2017).

[19] H. Park, A. K. L. Lim, A. P. Alivisatos, J. Park, and P. L. McEuen, Fabrication of metallic electrodes with nanometer separation by electromigration, Appl. Phys. Lett. **75**, 301 (1999).

[20] H. Park and P. L. McEuen, Nano-mechanical oscillations in a single-C_{60} transistor, Nature (London) **407**, 57 (2000).

[21] J. Park, A. N. Pasupathy, J. I. Goldsmith, C. Chang, Y. Yaish, J. R. Petta, M. Rinkoski, J. P. Sethna, H. D. Abruña, and P. L. McEuen, Coulomb blockade and the Kondo effect in single-atom transistors, Nature (London) **417**, 722 (2002).

[22] W. Liang, M. P. Shores, M. Bockrath, J. R. Long, and H. Park, Kondo resonance in a single-molecule transistor, Nature (London) **417**, 725 (2002).

[23] R. Vincent, S. Klyatskaya, M. Ruben, W. Wernsdorfer, and F. Balestro, Electronic read-out of a single nuclear spin using a molecular spin transistor, Nature (London) **488**, 357 (2012).

[24] C. B. Winkelmann, N. Roch, W. Wernsdorfer, V. Bouchiat, and F. Balestro, Superconductivity in a single-C_{60} transistor, Nat. Phys. **5**, 876 (2009).

[25] D. M. T. van Zanten, F. Balestro, H. Courtois, and C. B. Winkelmann, Probing hybridization of a single energy level coupled to superconducting leads, Phys. Rev. B **92**, 184501 (2015).

[26] D. M. T. van Zanten, D. M. Basko, I. M. Khaymovich, J. P. Pekola, H. Courtois, and C. B. Winkelmann, Single Quantum Level Electron Turnstile, Phys. Rev. Lett. **116**, 166801 (2016).

[27] See Supplemental Material http://link.aps.org/supplemental/10.1103/PhysRevResearch.2.012065, which includes Refs. [28–41], for a description of the sample fabrication process, electrical characterization, data for a second sample, theoretical modeling including NRG calculations, as well as the determination of Andreev bound state dispersions from renormalized perturbation theory.

[28] H. Krakauer, M. Posternak, and A. J. Freeman, Linearized augmented plane-wave method for the electronic band structure of thin films, Phys. Rev. B **19**, 1706 (1979).

[29] A. Ghosal, M. Randeria, and N. Trivedi, Role of Spatial Amplitude Fluctuations in Highly Disordered *s*-Wave Superconductors, Phys. Rev. Lett. **81**, 3940 (1998).

[30] J. M. Thijssen and H. S. J. Van der Zant, Charge transport and single-electron effects in nanoscale systems, Phys. Status Solidi B **245**, 1455 (2008).

[31] M.-S. Choi, M. Lee, K. Kang, and W. Belzig, Kondo effect and Josephson current through a quantum dot between two superconductors, Phys. Rev. B **70**, 020502 (2004).

[32] S. M. Cronenwett, T. H. Oosterkamp, and L. P. Kouwenhoven, A tunable Kondo effect in quantum dots, Science **281**, 540 (1998).

[33] E. J. H. Lee, X. Jiang, R. Žitko, R. Aguado, C. M. Lieber, and S. De Franceschi, Scaling of subgap excitations in a superconductor-semiconductor nanowire quantum dot, Phys. Rev. B **95**, 180502 (2017).

[34] D. Goldhaber-Gordon, J. Göres, M. A. Kastner, H. Shtrikman, D. Mahalu, and U. Meirav, From the Kondo Regime to the Mixed-Valence Regime in a Single-Electron Transistor, Phys. Rev. Lett. **81**, 5225 (1998).

[35] I. Affleck, J.-S. Caux, and A. M. Zagoskin, Andreev scattering and Josephson current in a one-dimensional electron liquid, Phys. Rev. B **62**, 1433 (2000).

[36] Y. Tanaka, A. Oguri, and A. C. Hewson, Kondo effect in asymmetric Josephson couplings through a quantum dot, New J. Phys. **9**, 115 (2007).

[37] E. Vecino, A. Martin-Rodero, and A. Levy Yeyati, Josephson current through a correlated quantum level: Andreev states and π junction behavior, Phys. Rev. B **68**, 035105 (2003).

[38] N. Wentzell, S. Florens, T. Meng, V. Meden, and S. Andergassen, Magnetoelectric spectroscopy of Andreev bound states in Josephson quantum dots, Phys. Rev. B **94**, 085151 (2016).

[39] N. A. Court, A. J. Ferguson, and R. G. Clark, Energy gap measurement of nanostructured aluminium thin films for single Cooper-pair devices, Supercond. Sci. Technol. **21**, 015013 (2007).

[40] F. Levy-Bertrand, T. Klein, T. Grenet, O. Dupré, A. Benoît, A. Bideaud, O. Bourrion, M. Calvo, A. Catalano, A. Gomez *et al.*, Electrodynamics of granular aluminum from superconductor

to insulator: Observation of collective superconducting modes, Phys. Rev. B **99**, 094506 (2019).

[41] A. A. Shanenko, M. D. Croitoru, and F. M. Peeters, Superconducting nanofilms: Andreev-type states induced by quantum confinement, Phys. Rev. B **78**, 054505 (2008).

[42] D. Goldhaber-Gordon, H. Shtrikman, D. Mahalu, D. Abusch-Magder, U. Meirav, and M. A. Kastner, Kondo effect in a single-electron transistor, Nature (London) **391**, 156 (1998).

[43] B. Dutta, D. Majidi, A. García-Corral, P. A. Erdman, S. Florens, T. A. Costi, H. Courtois, and C. B. Winkelmann, Direct probe of the Seebeck coefficient in a Kondo-correlated single-quantum-dot transistor, Nano Lett. **19**, 506 (2019).

[44] J. Bauer, A. Oguri, and A. C. Hewson, Spectral properties of locally correlated electrons in a Bardeen–Cooper–Schrieffer superconductor, J. Phys.: Condens. Matter **19**, 486211 (2007).

[45] R. Maurand, T. Meng, E. Bonet, S. Florens, L. Marty, and W. Wernsdorfer, First-Order 0-π Quantum Phase Transition in the Kondo Regime of a Superconducting Carbon-Nanotube Quantum Dot, Phys. Rev. X **2**, 011009 (2012).

[46] M. Ruby, F. Pientka, Y. Peng, F. von Oppen, B. W. Heinrich, and K. J. Franke, Tunneling Processes into Localized Subgap States in Superconductors, Phys. Rev. Lett. **115**, 087001 (2015).

[47] S.-H. Ji, T. Zhang, Y.-S. Fu, X. Chen, X.-C. Ma, J. Li, W.-H. Duan, J.-F. Jia, and Q.-K. Xue, High-Resolution Scanning Tunneling Spectroscopy of Magnetic Impurity Induced Bound States in the Superconducting Gap of Pb Thin Films, Phys. Rev. Lett. **100**, 226801 (2008).

[48] M. Ruby, Y. Peng, F. von Oppen, B. W. Heinrich, and K. J. Franke, Orbital Picture of Yu-Shiba-Rusinov Multiplets, Phys. Rev. Lett. **117**, 186801 (2016).

[49] D.-J. Choi, C. Rubio-Verdú, J. de Bruijckere, M. M. Ugeda, N. Lorente, and J. I. Pascual, Mapping the orbital structure of impurity bound states in a superconductor, Nat. Commun. **8**, 1 (2017).

[50] A. Zazunov, V. S. Shumeiko, E. N. Bratus, J. Lantz, and G. Wendin, Andreev Level Qubit, Phys. Rev. Lett. **90**, 087003 (2003).

[51] C. Buizert, A. Oiwa, K. Shibata, K. Hirakawa, and S. Tarucha, Kondo Universal Scaling for a Quantum Dot Coupled to Superconducting Leads, Phys. Rev. Lett. **99**, 136806 (2007).

[52] J. Bauer, J. I. Pascual, and K. J. Franke, Microscopic resolution of the interplay of Kondo screening and superconducting pairing: Mn-phthalocyanine molecules adsorbed on superconducting Pb (111), Phys. Rev. B **87**, 075125 (2013).

[53] V. Meden, The Anderson-Josephson quantum dot–A theory perspective, J. Phys.: Condens. Matter **31**, 163001 (2019).

[54] T. Meng, S. Florens, and P. Simon, Self-consistent description of Andreev bound states in Josephson quantum dot devices, Phys. Rev. B **79**, 224521 (2009).

[55] A. Anthore, H. Pothier, and D. Estève, Density of States in a Superconductor Carrying a Supercurrent, Phys. Rev. Lett. **90**, 127001 (2003).